9542 *Biochemistry* **2009,** *48,* 9542–9555
DOI: 10.1021/bi901056a

BIOCHEMISTRY
including biophysical chemistry & molecular biology
Article

Factors That Affect Oxygen Activation and Coupling of the Two Redox Cycles in the Aromatization Reaction Catalyzed by NikD, an Unusual Amino Acid Oxidase[†,‡]

Phaneeswara-Rao Kommoju,[§,⊥] Robert C. Bruckner,[§,⊥] Patricia Ferreira,[§] Christopher J. Carrell,[∥] F. Scott Mathews,[∥] and Marilyn Schuman Jorns*[,§]

[§]*Department of Biochemistry and Molecular Biology, Drexel University College of Medicine, Philadelphia, Pennsylvania 19102, and* [∥]*Department of Biochemistry and Molecular Biophysics, Washington University School of Medicine, St. Louis, Missouri 63110* [⊥]*These authors contributed equally to this work.*

Received June 22, 2009; Revised Manuscript Received July 28, 2009

ABSTRACT: NikD is a flavoprotein oxidase that catalyzes the oxidation of piperideine-2-carboxylate (P2C) to picolinate in a remarkable aromatization reaction comprising two redox cycles and at least one isomerization step. Tyr258 forms part of an "aromatic cage" that surrounds the ring in picolinate and its precursors. Mutation of Tyr258 to Phe does not perturb the structure of nikD but does affect the coupling of the two redox cycles and causes a 10-fold decrease in turnover rate. Tyr258Phe catalyzes a quantitative two-electron oxidation of P2C, but only 60% of the resulting dihydropicolinate intermediate undergoes a second redox cycle to produce picolinate. The mutation does not affect product yield with an alternate substrate (3,4-dehydro-L-proline) that is aromatized in a single two-electron oxidation step. Wild-type and mutant enzymes exhibit identical rate constants for oxidation of P2C to dihydropicolinate and isomerization of a reduced enzyme·dihydropicolinate complex. The observed rates are 200- and 10-fold faster, respectively, than the mutant turnover rate. Release of picolinate from Tyr258Phe is 100-fold faster than turnover. The presence of a bound substrate or product is a key factor in oxygen activation by wild-type nikD, as judged by the 10−75-fold faster rates observed for complexes of the reduced enzyme with picolinate, benzoate, or 1-cyclohexenoate, a 1-deaza-P2C analogue. The reduced Tyr258Phe·1-cyclohexenoate complex is 25-fold less reactive with oxygen than the wild-type complex. We postulate that mutation of Tyr258 causes subtle changes in active site dynamics that promote release of the reactive dihydropicolinate intermediate and disrupt the efficient synchronization of oxygen activation observed with wild-type nikD.

NikD, an unusual flavoprotein oxidase, catalyzes a remarkable aromatization reaction involving two redox cycles and plays a critical role in the biosynthesis of nikkomycin antibiotics. Nikkomycins are potent antifungal agents that block cell wall formation by inhibiting the biosynthesis of chitin, the second most abundant polysaccharide in nature (*2*, *3*). Nikkomycins contain a nonribosomal peptide linked by a peptide bond to a nucleoside moiety. The nonribosomal peptide contains an essential N-terminal pyridyl residue that is derived from L-lysine via a two-step pathway mediated by nikD and an L-lysine-α-aminotransferase. The α-aminotransferase converts L-lysine to piperideine-2-carboxylate (P2C)[1] (*4*), a compound that can exist in imine and enamine tautomeric forms (*5*−*7*). NikD catalyzes a four-electron oxidation of P2C to picolinate, accompanied by the reduction of 2 mol of oxygen to hydrogen peroxide (*8*) (Scheme 1). The enzyme contains 1 mol of covalently bound FAD (*9*), acts as an obligate two-electron acceptor (*8*), and exhibits sequence and structural homology with monomeric sarcosine oxidase (MSOX) and other members of a family of amino acid oxidases that contain a single covalently bound flavin (*10*−*16*).

NikD exhibits two unique structural features as compared with other members of the MSOX family of amino acid oxidases (*10*). First, nikD contains a mobile cation-binding loop of unknown function that has been shown to bind sodium or potassium ions. Second, nikD exhibits two distinct modes for substrate binding, as judged by the open and closed forms of the enzyme·picolinate complex. In the closed form, picolinate is bound parallel with the flavin ring, the indole ring of Trp355 is perpendicular to the flavin ring, and the active site is inaccessible to solvent. This ligand binding mode is compatible with redox catalysis and similar to that observed with MSOX. In the open form, picolinate is bound perpendicular to the flavin ring, Trp355 is stacked atop the flavin ring, and the active site is accessible to solvent. This binding mode is not compatible with redox catalysis or observed with MSOX. However, the coplanar orientation of the flavin and indole rings is required for charge-transfer interaction between FAD and Trp355, a feature observed with solutions of the ligand-free enzyme at weakly alkaline pH (*9*, *17*).

The nikD-catalyzed oxidation of P2C to picolinate proceeds via a reduced enzyme·dihydropicolinate (DHP) intermediate. There are six possible DHP isomers. Stopped-flow studies show

[†]This work was supported in part by Grant AI 55590 (M.S.J.) from the National Institutes of Health.

[‡]The atomic coordinates for the crystal structure of the Tyr258Phe mutant form of nikD can be accessed through the RCSB Protein Data Bank as entry 3HZL.

*To whom correspondence should be addressed. Phone: (215) 762-7495, Fax: (215) 762-4452. E-mail: marilyn.jorns@drexelmed.edu.

[1]Abbreviations: FAD, flavin adenine dinucleotide; P2C, piperideine-2-carboxylate; CHA, 1-cyclohexenoate; ES complex, enzyme·substrate complex; MSOX, monomeric sarcosine oxidase; DHP, dihydropicolinate; MPD, 2-methyl-2,4-pentanediol.

 Published on Web 08/24/2009

Scheme 1: NikD-Catalyzed Four-Electron Oxidation of P2C to Picolinate

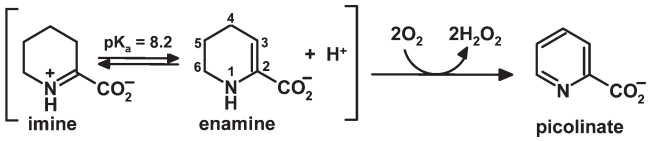

that nikD oxidizes the electron-rich enamine tautomer of P2C, a result that eliminates three possible DHP isomers (*18*). Recent mutagenesis studies rule out the only possible candidates (Glu101 and Asp276) for a catalytic base in the initial two-electron oxidation step (*17*). This outcome provides compelling evidence that nikD oxidizes the bond between N(1) and C(6) in the enamine tautomer to produce DHP isomer A (Scheme 2), ruling out alternate paths that require an active site base to mediate the oxidation of a carbon−carbon bond. Because the same restraint applies to the second two-electron oxidation step, picolinate formation must be accomplished by a pathway that does not involve oxidation of a carbon−carbon bond in DHP.

A relatively slow phase is observed after formation of the reduced enzyme·DHP complex that appears to be rate-determining during turnover. Importantly, the slow phase exhibits a kinetic isotope effect when [4,4,5,5,6,6-D$_6$]P2C is used as the substrate, indicating that the slow phase must involve cleavage of one or more C−H bonds in DHP isomer A (*18*). DHP isomer A can be converted to DHP isomer B in a two-step process involving the intermediate formation of DHP isomer C (Scheme 2). We recently proposed a novel role for reduced FAD as the acid−base catalyst that is required for the postulated isomerization of the reduced enzyme·DHP complex (*17*). DHP isomer B contains an oxidizable carbon−nitrogen bond between N(1) and C(6) and can be converted to picolinate in a reaction similar to that observed with the enamine tautomer of P2C. In principle, DHP isomer C might also be converted to picolinate in a reaction that is functionally equivalent to the direct oxidation of the N(1)−C(6) bond in isomer B, but this option requires a 180° "flip" of the intermediate to place the C(4)H group in isomer C in a position favorable for hydride transfer to FAD N(5) (*10*). The required reorientation of isomer C cannot occur within a "closed complex" where ligand movement is restricted by hydrogen bonding to the ligand carboxylate and a "cage" of aromatic residues that surrounds the ligand ring but might be achieved by the transient formation of an "open complex".

Steady-state kinetic studies indicate that oxygen reacts with a reduced enzyme·DHP complex to produce an oxidized complex that can undergo a second redox cycle, completing the aromatization process (*18*). It is known that P2C oxidation occurs on the *re* face of the flavin ring (*10*), but the site and mechanism of oxygen activation are unknown. Studies with MSOX show that amino acid substrate oxidation and oxygen reduction occur on opposite faces of the flavin ring. A single basic residue, Lys265, on the *si* face of the flavin ring has been identified as the site of oxygen activation in MSOX (*19*). Puzzlingly, Lys265 is neither conserved nor conservatively substituted in nikD, unlike other MSOX homologues, suggesting that other factors must be responsible for the activation of oxygen by nikD.

Tyr258 forms part of an "aromatic cage" that surrounds the ligand ring in the enzyme·picolinate complex. The residue was mutated as part of a study designed to determine the identity of an unknown ionizable residue (pK_a = 7.3) that when protonated eliminates charge-transfer interaction between FAD and Trp355 (*9*, *17*). A catalytic role for Tyr258 is not obvious on the basis of observed crystal structures because the side chain points away from the ligand in both the closed and open forms. In this paper, we report unexpected effects of a conservative mutation of Tyr258 on the coupling of the two redox cycles in the aromatization of P2C and identify parameters that affect the activation of oxygen by nikD.

Scheme 2: Two Possible Mechanisms for the Conversion of P2C to Picolinate[a]

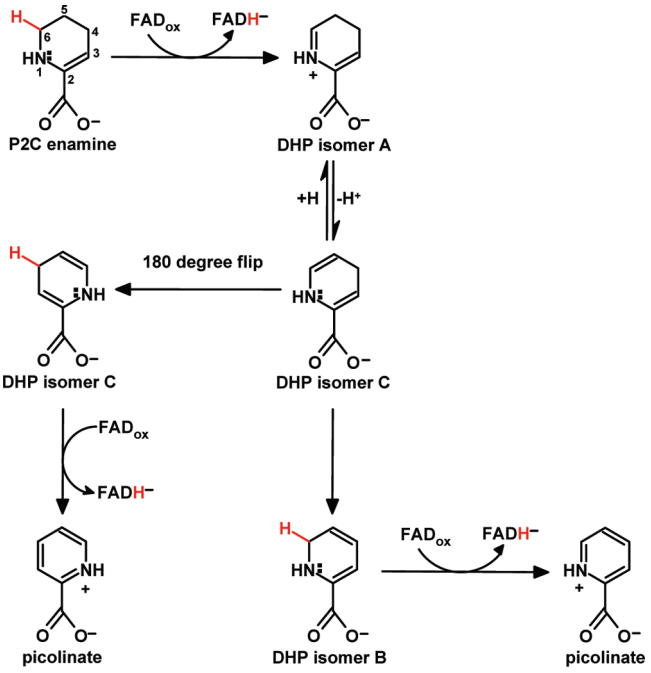

[a]For each redox step, the hydride equivalent transferred to FAD is colored red. Reduced FAD is postulated to function as an acid−base catalyst in the isomerization steps (*17*) (not shown). Briefly, the N(5)H group in FADH$^-$ is proposed to be the proton acceptor required for conversion of DHP isomer A to DHP isomer C; the N(5)H$_2^+$ and C(4)O groups in FADH$_2$ are postulated to act as the proton donor and acceptor, respectively, in the conversion of DHP isomer C to DHP isomer B. The 180° flip of DHP isomer C would require the transient formation of an "open complex", as discussed in the text.

EXPERIMENTAL PROCEDURES

Materials. Catalase, horseradish peroxidase, and *o*-dianisidine were purchased from Sigma. Amplex Red was obtained from Invitrogen. 3,4-Dehydro-L-proline was obtained from BaChem. Benzoic acid was purchased from Fisher. 1-Cyclohexenoate was obtained from Aldrich. P2C was prepared as described by Bruckner et al. (*8*). Restriction enzymes and T4 DNA ligase were purchased from New England Biolabs. *Pfu* DNA polymerase was obtained from Stratagene.

Mutation of Tyr258 to Phe. Polymerase chain reactions (PCRs) were conducted using a Hybaid Touchdown Thermocycler or a Perkin-Elmer 9600 GeneAmp PCR System. Products were purified as previously described (*20*). Mutations were generated by using the overlap extension PCR method described by Ho et al. (*21*) and plasmid pDV101 (*9*) as a template. The left-hand fragment was generated using START (external primer) as the forward primer and an internal backward primer containing the desired mutation (Table 1). The right-hand fragment was generated using an internal forward primer containing the desired mutation and END (external primer) as the backward

Table 1: Primers Used for Mutagenesis[a]

primer type	forward	backward
external	START (5′-GACTCACTATAGGGAGACC ACAACGGTTTCCCTCTAG-3′)	END (5′-GTCGCCACCGTCGTCGGTTGA GTCGAAGGAAAGCCC-3′)
internal		
Tyr278Phe	5′-CAACCTGTTCTtcGGGTTCGGCCAC-3′	5′-GTTGGACAAGAagCCCAAGCCGGTG-3′

[a]Mutagenic sites in the primers are shown in lowercase; the codon targeted for mutagenesis is underlined.

primer. The purified left- and right-hand fragments were combined using START and END as forward and backward primers, respectively. The final PCR product was purified, digested with *Nde*I and *Xho*I, purified again, and then subcloned between the *Nde*I and *Xho*I sites of plasmid pET23a. The resulting construct was used to transform *Escherichia coli* BL21(DE3) cells to ampicillin resistance. For screening, plasmid DNA was isolated from randomly selected clones and digested with *Nde*I and *Xho*I. A plasmid that exhibited the expected insert size (Y258F pGPZ19) was isolated and sequenced across the entire insert. Sequencing was conducted by MWG Biotech.

Enzyme Isolation. Recombinant wild-type nikD and Tyr258Phe were isolated from cells grown in Terrific Broth and purified as previously described (*9*). Both preparations contained a trace amount of catalase that affected the yield of hydrogen peroxide obtained in turnover studies with substrate amounts of enzyme. Catalase-free preparations for these studies were obtained by ultrafiltration using a Microcon Ultracel YM-100 concentrator to remove the higher-molecular weight catalase contaminant. The contaminant did not affect initial rate measurements conducted using catalytic amounts of enzyme in a continuous horseradish peroxidase-coupled assay, as judged by control studies with catalase-free and unfiltered preparations.

Crystallization and Data Collection. Crystals of the Tyr258Phe mutant protein were obtained by the sitting drop vapor diffusion method (*22*). After the protein was first exchanged with 10 mM TRIS buffer (pH 7.6) and concentrated to 10 or 20 mg/mL using a Centricon 30 membrane filter, 4 mL of Tyr258Phe (at 10 mg/mL) was mixed with 4 mL of 20−30% 2-methyl-2,4-pentanediol (MPD) in 100 mM MES buffer (pH 5.7). The crystals were bright yellow and formed plates ~200 μm × 150 μm × 20 μm in size. They are monoclinic in space group *C*2 with the following cell dimensions: a = 88.39 Å, b = 90.53 Å, c = 85.97 Å, and β = 118.36°.

Diffraction data were collected from a crystal that was transferred using a nylon loop directly from a crystallization drop to a cryostream of nitrogen gas at 110 K after removal of excess mother liquor from the crystal surface. Data were collected on an ADSC Quantum-4 CCD instrument at beamline 14-BM-C at BIOCARS (Argonne, IL). A single pass of 180° with steps of 0.25° was sufficient to collect a complete data set to 1.55 Å resolution. Scaling and merging of the data were conducted using HKL2000 (*23*).

Phasing and Refinement. The structure of the Tyr258Phe mutant form of nikD was determined by molecular replacement using CNS. The refined coordinates of the open form of wild-type nikD [Protein Data Bank (PDB) entry 2OLO] were used as a search model. Refinement was conducted by a round of simulated annealing in CNS, followed by alternating rounds of atomic refinement in CNS and model building in XTALVIEW (*24*). The refinement statistics can be found in Table 2.

Enzyme Assays and Steady-State Kinetic Studies. Enzyme assays were conducted at 25 °C in 100 mM potassium phosphate buffer (pH 8.0) containing variable concentrations of P2C and oxygen, as indicated. In direct assays, picolinate formation was monitored at 264 nm (ε = 3980 M^{-1} cm^{-1}) (*8*). For coupled assays, the reaction mixture included 6 units/mL horseradish peroxidase and 320 μM *o*-dianisidine or 200 μM Amplex Red. Reactions with *o*-dianisidine or Amplex Red as the chromogenic substrate were monitored at 460 nm (ε = 6765 M^{-1} cm^{-1}) or 563 nm (ε = 52200 M^{-1} cm^{-1}), respectively (*9*, *25*, *26*). Steady-state kinetic studies were conducted using the horseradish peroxidase-coupled assay with Amplex Red. Reaction mixtures were equilibrated with water-saturated gas mixtures containing 10, 21, 44, or 100% oxygen (balance nitrogen), as previously

Table 2: Data Collection and Refinement Statistics

Data Collection	
wavelength (Å)	0.9000
resolution range (Å)[a]	1.55 (1.59−1.55)
no. of reflections	532331
no. of unique reflections	86058
R_{merge} (%)[b]	6.5 (40.1)
completeness (%)	99.6 (97.4)
$\langle I/\sigma(I)\rangle$[c]	27.1 (3.0)
redundancy	6.2 (4.5)
Refinement	
resolution range (Å)	50−1.55
R_{work}[d]	0.208
R_{free}[e]	0.225
no. of protein atoms	3089
no. of FAD atoms	53
no. of ligand atoms	9
no. of other atoms[f]	24
no. of water molecules	416
B-factor (Å^2)	
protein	25.3
FAD	16.1
ligands	26.7
MPD	40.3
water	35.5
root-mean-square deviation	
bonds (Å)	0.014
angles (deg)	1.73
ΔB main−main (Å^2)	1.8
ΔB side−side (Å^2)	2.7
ΔB main−side (Å^2)	2.0
Ramachandran plot (%)	
most favored	91.6
additional allowed	8.4
generously allowed	0

[a]Values in parentheses refer to the highest-resolution shell. [b]$R_{merge}(I) = \sum|I_i - \langle I\rangle|/\sum I_i$, where I_i is the intensity of the ith observation, $\langle I\rangle$ is the mean intensity of the reflection, and the summation extends over all data. [c]$I/\sigma(I)$ is the average signal-to-noise ratio for merged reflection intensities. [d]*R*-factor = $\sum||F_o| - |F_c||/\sum|F_o|$, where $|F_o|$ is the observed structure factor amplitude, $|F_c|$ is the calculated structure factor amplitude, and the summation extends over all data. [e]R_{free} is the *R*-factor obtained for a test set of reflections, consisting of a randomly selected 5% subset of the diffraction data, not used during refinement. [f]The structure contains three molecules of MPD.

Table 3: Spectral Properties of Tyr258Phe and Wild-Type NikD[a]

	wild type	Tyr258Phe
absorption maxima (nm)	379, 456[b]	376, 455
ε_{550} (M^{-1} cm^{-1})	1240	1270
$\varepsilon_{\lambda_{max}}$[c] ($M^{-1}$ cm^{-1})	11200[b]	10400
$A_{280}/A_{\lambda_{max}}$[c]	8.77−13.0[d]	9.16
mol of FAD/mol of protein	0.54−0.90[d]	0.89
spectral pK_a	7.31 ± 0.03[e]	7.2 ± 0.1

[a]Spectral properties were determined in 100 mM potassium phosphate buffer (pH 8.0) at 25 °C, except for pH titrations where the pH of the buffer was varied. [b]Data previously reported (*9*). [c]λ_{max} = 456 nm (wild type) or 455 nm (Tyr258Phe). [d]Data previously reported (*20*). [e]Data previously reported (*17*).

described (*18*). Steady-state kinetic parameters were estimated by fitting eq 1 to the data.

$$v = \frac{v_{max}[A][B]}{K_{ia}K_b + K_a[B] + K_b[A] + [A][B]} \quad (1)$$

Steady-State Spectroscopy. An Agilent Technologies 8453 diode array spectrometer was used to record absorption spectra. Anaerobic spectral experiments were conducted as previously described (*27*). The concentration of mutant or wild-type enzyme was determined at pH 8.0 using the extinction coefficients listed in Table 3. Extinction coefficients of oxidized Tyr258Phe and the stoichiometry of covalent flavin incorporation were determined after denaturation with 3 M guanidine hydrochloride, as previously described (*15*). The change in the extinction coefficient of wild-type nikD or Tyr258Phe at 264 nm upon reduction ($\Delta\varepsilon_{reduced-oxidized}$) was determined after anaerobic reaction of the enzyme with a 2- or 1.2-fold molar excess, respectively, of P2C in 100 mM potassium phosphate buffer (pH 8.0) at 25 °C under anaerobic conditions. Turnover of wild-type nikD or Tyr258Phe with 3,4-dehydro-L-proline was measured by monitoring the formation of pyrrole-2-carboxylate at 256 nm (ε = 12400 M^{-1} cm^{-1}) (*8*) in 100 mM potassium phosphate buffer (pH 8.0) containing 1.29 mM oxygen at 25 °C. Dissociation constants for complexes formed with Tyr258Phe and picolinate or 1-cyclohexenoate were determined by fitting an equation for a tight binding inhibitor (eq 2)

$$\Delta A = \frac{\Delta A_{max}}{2E_T}\left[X_T + E_T + K_d - \sqrt{(X_T + E_T + K_d)^2 - 4E_T X_T}\right] \quad (2)$$

where X_T and E_T are total ligand and enzyme concentrations, respectively) to the data. Spectra corresponding to 100% complex formation were calculated as previously described (*28*). A pH titration of Tyr258Phe was conducted as detailed in the legend of Figure 2. Fitting of binding or pH titration equations was conducted by using Sigma Plot 10 (Systat Software).

Rapid Reaction Spectroscopy. Rapid reaction kinetic measurements were performed by using a Hi-Tech Scientific SF-61DX2 stopped-flow spectrometer (dead time of 1.7 ms). Data were collected in log mode to maximize the number of points acquired during the early phase of each reaction. All spectra or single-wavelength kinetic traces are the averages of at least three replicate shots. Reductive half-reactions with Tyr258Phe and P2C were monitored by using diode array detection in anaerobic 100 mM potassium phosphate buffer (pH 8.0) containing 50 mM glucose and glucose oxidase (14.7 units/mL). Tonometers containing enzyme or substrate and the entire flow circuit of the stopped-flow spectrometer were made anaerobic by multiple cycles of evacuation and flushing with oxygen-scrubbed argon in conjunction with a glucose/glucose oxidase system, as previously described (*18*). Spectra are corrected for a small spectral contribution from P2C in the near-ultraviolet region. The integration time for each spectrum is 1.5 ms; the indicated time for each spectrum is after the collection of data has been triggered. The kinetics of binding of 1-cyclohexenoate or picolinate to Tyr258Phe were monitored in aerobic 100 mM potassium phosphate buffer (pH 8.0) at 25 °C by using photomultiplier detection. To prepare free reduced enzyme for oxidative half-reaction studies, 100 mM potassium phosphate buffer (pH 8.0) containing 1 equiv of 3,4-dehydro-L-proline was placed in the main compartment of a tonometer and a concentrated aliquot of wild-type nikD or Tyr258Phe was placed in a side arm. The solutions were made anaerobic as described above, except for the glucose/glucose oxidase system which could not be used in these experiments. Instead, traces of residual oxygen were removed by bubbling oxygen-scrubbed argon gas through the buffer in the main compartment and over the surface of the enzyme in the side arm. The enzyme was then tipped into the main compartment of the tonometer and incubated for 3.5 h at room temperature to ensure complete reduction. To prepare reduced enzyme complexes, an aliquot of an anaerobic solution of the desired ligand in the same buffer was anaerobically transferred to the tonometer containing the reduced enzyme. Solutions containing free reduced enzyme were mixed (1:1) in the stopped-flow spectrometer with 100 mM potassium phosphate buffer (pH 8.0) that had been equilibrated with water-saturated gas mixtures containing 21.0, 44.0, 65.0, or 100% oxygen (balance nitrogen). For reactions with reduced enzyme complexes, the indicated ligand was added at the same concentration to the aerobic buffer solutions. The spectrophotometer was operated in diode array mode. To minimize the exposure of the sample to the light, an automatic shutter was used for reactions lasting more than 30 s. Fitting of single-wavelength kinetic traces was conducted by using Sigma Plot 10 (Systat Software), KinetAsyst 3 (TgK Scientifc), or Kinetic Studio (TgK Scientific).

RESULTS

Crystal Structure of Tyr258Phe. Crystals of the open form of the Tyr258Phe complex with picolinate were obtained to determine whether the mutation affected the structure of nikD. The root-mean-square deviation for Cα atoms between the structures of the mutant complex (resolution of 1.55 Å) and the corresponding wild-type complex (resolution of 1.90 Å) is 0.24 Å. The results indicate that, within experimental error, the structures are identical at the fold level. FAD in Tyr258Phe is covalently attached to Cys321, as observed with wild-type nikD. A close-up inspection of the area above the *re* face of the flavin ring shows virtual superimposition of the picolinate ligand, Phe258/Tyr258, and other active site residues in the mutant and wild-type structures (Figure 1). A similar correspondence is observed for residues on the opposite *si* face of the flavin ring and in a loop (Gly259−Val271) which binds monovalent cations (Na^+ and K^+) in the closed form (*10*).

Spectral Properties of Tyr258Phe. Very similar absorption spectra are observed at pH 8.0 with Tyr258Phe and wild-type nikD (Figure 2A and Table 3). Both preparations exhibit two characteristic flavin absorption maxima at λ > 300 nm and a long-wavelength absorption band that can be attributed to charge-transfer interaction with Trp355 (*20*). Negligible

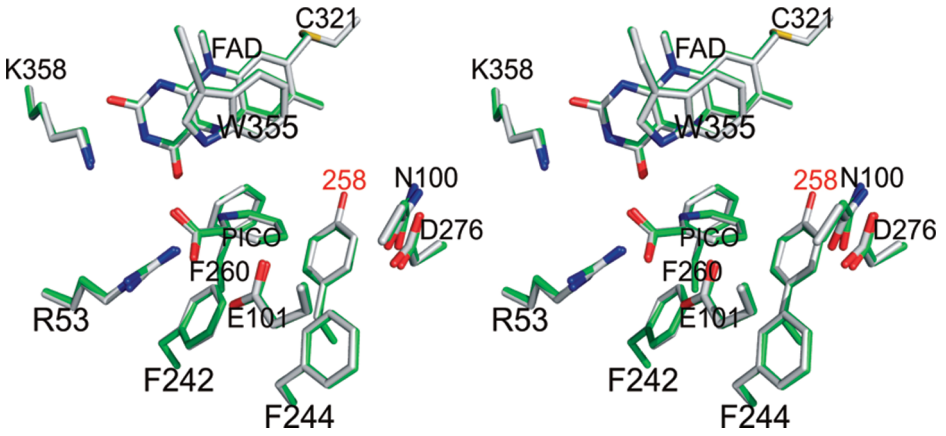

FIGURE 1: Stereoview comparison of the active site in the open form of Tyr258Phe or wild-type nikD (PDB entry 2OLO) in complex with picolinate (PICO). Carbon atoms are colored green in the Tyr258Phe complex or white in the wild-type complex. In both structures, oxygens are colored red, nitrogens are colored blue, and the sulfur is colored yellow. The diagram was rendered using PYMOL (http://www.pymol.org).

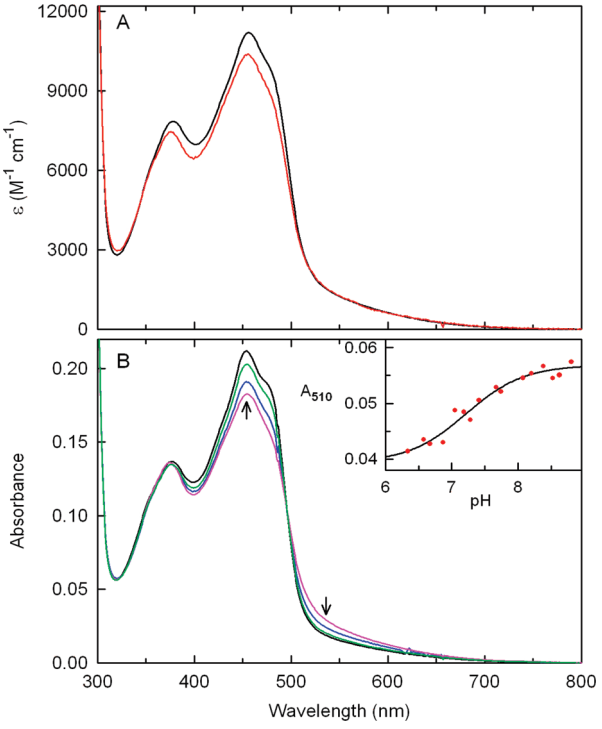

FIGURE 2: Spectral properties of Tyr258Phe. Spectra were recorded at 25 °C in 100 mM potassium phosphate buffer at the indicated pH. Panel A compares absorption spectra observed with Tyr258Phe (red curve) and wild-type nikD (black curve) at pH 8.0. Panel B shows the effect of pH on the absorption spectrum of Tyr258Phe. The black, green, blue, and magenta curves were recorded at pH 6.34, 6.58, 7.05, and 8.38, respectively. The arrows indicate the direction of spectral change observed when the pH is decreased. The inset shows a plot of the absorbance at 510 nm as a function of pH. The solid black line was obtained by fitting a theoretical pH titration curve [$Y = (AH^+ + BK_a)/(H^+ + K_a)$] to the data (red circles).

long-wavelength absorbance is observed with solutions of Tyr258Phe at pH 6.3, similar to that of wild-type nikD (*9*, *17*). Increasing the pH from 6.3 to 9.0 results in the recovery of the mutant charge-transfer band, accompanied by a decrease in absorbance at 456 nm (Figure 2B). Analysis of the absorbance increase at 510 nm as a function of pH provides evidence of a single ionizable group with a pK_a of 7.2 ± 0.1 (Figure 2B, inset). The observed pK_a is, within experimental error, identical to a value obtained with wild-type nikD (pK_a = 7.31 ± 0.01) (*17*).

Scheme 3: A Minimal Steady-State Kinetic Mechanism for the NikD-Catalyzed Conversion of P2C to Picolinate (P)[a]

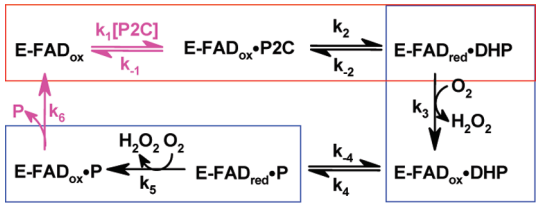

[a]The red box indicates the portion of the overall reaction that is monitored in reductive half-reaction studies. The blue boxes indicate portions of the overall reaction that are monitored or modeled in oxidative half-reaction studies. Magenta arrows indicate product release or substrate binding steps that are probed in thermodynamic or kinetic studies with picolinate or a P2C analogue, respectively.

The results rule out Tyr258 as a possible candidate for the unknown ionizable residue in wild-type nikD.

Does the Tyr258Phe Mutation Affect the Rate of Aerobic Turnover with P2C?. Steady-state kinetic analysis of the reaction of Tyr258Phe with P2C was measured by monitoring hydrogen peroxide formation using a sensitive horseradish peroxidase-coupled assay with Amplex Red (ε_{563} = 52200 M^{-1} cm^{-1}) as the chromogenic substrate (*26*). Double-reciprocal plots of reaction rate versus P2C concentration at different oxygen concentrations or versus oxygen concentration at different P2C concentrations are linear and intersect to the left of the *Y*-axis, below the *X*-axis (data not shown) (see Figure S1 of the Supporting Information). The results are consistent with a sequential mechanism in which oxygen reacts with a reduced enzyme·DHP complex to yield an oxidized enzyme·DHP complex that may undergo a second redox cycle to produce picolinate (Scheme 3), as observed with wild-type nikD (*18*). The steady-state kinetic parameters listed in Table 4 were obtained by fitting an equation for a sequential mechanism (eq 1) to the data. The apparent second-order rate constant for the reaction of the oxidized mutant enzyme with P2C ($k_{cat}/K_{m,P2C}$) is 50-fold slower than that observed with wild-type nikD. The reaction of the reduced mutant enzyme with oxygen is 20-fold slower than the wild-type reaction, as estimated on the basis of values obtained for $k_{cat}/K_{m,oxygen}$. The turnover rate of the mutant at saturating oxygen and P2C concentrations is 10-fold slower than that of the wild-type enzyme.

Table 4: Kinetic Parameters for the Reaction of Tyr258Phe or Wild-Type NikD with P2C at pH 8.0 and 25 °C

	reductive half-reaction[a]				steady-state turnover[b]		
preparation	k_{lim} (s^{-1})	k_{slow} (s^{-1})	$K_{d,app}$ (μM)	$k_{lim}/K_{d,app}$ (M^{-1} s^{-1})	k_{cat} (s^{-1})	$k_{cat}/K_{m,P2C}$ (M^{-1} s^{-1})	$k_{cat}/K_{m,oxygen}$ (M^{-1} s^{-1})
Tyr258Phe	54 ± 1	2.78 ± 0.08	250 ± 30	(2.2 ± 0.2) × 10^5	0.26 ± 0.03	(3.7 ± 0.7) × 10^3	(1.2 ± 0.2) × 10^2
wild type[c]	53 ± 1	2.7 ± 0.1	260 ± 20	(2.0 ± 0.2) × 10^5	2.3 ± 0.2	(2.0 ± 0.3) × 10^5	(2.6 ± 0.2) × 10^3

[a]The reductive half-reaction, as monitored at 456 nm, exhibits three phases: (1) an initial lag, (2) a rapid decrease in absorbance (k_{fast}) that exhibits a hyperbolic dependence on the concentration of P2C [$k_{obs} = k_{lim}$[P2C]/($K_{d,app}$ + [P2C])], and (3) a slow decrease in absorbance (k_{slow}) that is independent of the concentration of P2C. Values for k_{fast} and k_{slow} were obtained by fitting a double-exponential equation ($y = Ae^{-k_{fast}t} + Be^{-k_{slow}t} + C$) to the observed decrease in absorbance at 456 nm (phases 2 and 3). [b]Double-reciprocal plots obtained with wild-type nikD or Tyr258Phe exhibit intersecting lines ($K_{i,P2C}$ = 2.9 ± 0.8 or 4 ± 2 μM, respectively). Values for k_{cat} were calculated on the basis of the number of moles of picolinate per mole of enzyme per second. [c]Values for wild-type nikD from ref *18*.

Table 5: Initial Rates of Picolinate or Hydrogen Peroxide Formation during Turnover of Wild-Type NikD or Tyr258Phe with P2C[a]

			k_{obs} (min^{-1})			
				hydrogen peroxide		
enzyme	[O_2] (mM)	[P2C] (μM)	picolinate	*o*-dianisidine	Amplex Red	$k_{hydrogen\ peroxide}/k_{picolinate}$
Tyr258Phe	0.27	150	1.63 ± 0.02	3.5 ± 0.2	3.58 ± 0.06	2.1 ± 0.1,[b] 2.20 ± 0.05[c]
wild type	0.27	150	33 ± 1			
Tyr258Phe	1.29	20	3.05 ± 0.08	6.6 ± 0.1		2.16 ± 0.07[b]
wild type	1.29	20	45.2 ± 0.6	87.5 ± 0.3		1.94 ± 0.03[b]
Tyr258Phe	1.29	saturating[d]	5.96 ± 0.08		12.6 ± 0.3	2.11 ± 0.06[c]
wild type	1.29	saturating[d]	79 ± 3			

[a]Initial rates were measured in 100 mM potassium phosphate buffer (pH 8.0) at 25 °C by monitoring picolinate formation or in a horseradish peroxidase-coupled assay using *o*-dianisidine or Amplex Red as the chromogenic substrate, as detailed in Experimental Procedures. [b]Hydrogen peroxide determined using *o*-dianisidine as the chromogenic substrate. [c]Hydrogen peroxide determined using Amplex Red as the chromogenic substrate. [d]Values for $k_{cat,app}$ with Tyr258Phe or wild-type nikD were obtained by fitting a hyperbolic equation [$k_{obs} = (k_{cat,app}$[P2C])/($K_{m,app}$ + [P2C])] to initial rates observed with 5−150 or 6−150 μM P2C, respectively.

Turnover of wild-type nikD with P2C is typically measured using a less sensitive direct assay in which picolinate formation is monitored at 264 nm (ε_{264} = 3980 M^{-1} cm^{-1}) (*8*, *20*). Unlike that of the wild-type enzyme (*18*), the low activity of Tyr258Phe precluded a complete steady-state kinetic analysis using the direct assay. However, initial rates of picolinate formation with the mutant enzyme could be measured using a relatively high P2C concentration (150 μM) in air-saturated buffer (0.27 mM oxygen) or over a wider range of P2C concentrations in buffer saturated with 100% oxygen (1.29 mM). Under these conditions, initial rates of picolinate formation observed with the mutant enzyme are less than 10% of those observed with wild-type nikD (Table 5). We also measured initial rates of hydrogen peroxide formation within the range of substrate concentrations accessible with Tyr258Phe using a horseradish peroxidase-coupled assay with Amplex Red or *o*-dianisidine as the chromogenic substrate (*9*, *25*, *26*). Under all conditions tested, the initial rate of hydrogen peroxide formation observed with the mutant enzyme is 2-fold greater than the corresponding rate observed for picolinate formation (Table 5), as expected for a four-electron oxidation of P2C.

Does the Tyr258Phe Mutation Affect the Stoichiometry of Picolinate Formation?. The 2-fold difference in initial rates observed for hydrogen peroxide and picolinate formation suggested that Tyr258Phe would catalyze the quantitative conversion of P2C to picolinate, as observed with wild-type nikD (*8*). To test this prediction, we measured the amount of picolinate formed upon aerobic reaction of substrate amounts of Tyr258Phe (4−6 μM) with a modest excess of P2C (20 μM). The selected conditions allowed us to monitor both the redox state of the enzyme at 456 nm and formation of picolinate at 264 nm in reactions that could be followed to completion within a relatively short period of time.

Nearly complete reduction (95%) of Tyr258Phe is observed immediately after the enzyme is mixed with P2C in air-saturated buffer, as estimated by comparison of the observed ΔA_{456} with that expected for the fully reduced enzyme. The mutant remains reduced during the steady state. This indicates that enzyme reduction is faster than the reaction of the reduced enzyme with oxygen. The appearance of oxidized enzyme, as signaled by an increase in absorption at 456 nm, indicates that the reaction is apparently complete within 180 s (Figure 3A, trace 1).

Reduction of nikD results in an increase in the extinction coefficient of the enzyme at 264 nm, as judged by values obtained for $\Delta\varepsilon_{264}$ with Tyr258Phe or wild-type nikD ($\Delta\varepsilon_{264}$ = 10000 or 8100 M^{-1} cm^{-1}, respectively). The increase in absorbance at 264 nm observed immediately after Tyr258Phe is mixed with P2C (Figure 3A, trace 2) is largely (70%) attributable to enzyme reduction. The observed ΔA_{264} reaches a maximum 50 s after mixing and then decreases due to oxidation of reduced Tyr258Phe. The product formed in the mutant reaction exhibits a UV absorption spectrum characteristic of picolinate, as observed with wild-type nikD (Figure 3B). The amount of picolinate formed in each reaction was determined on the basis of the final observed ΔA_{264} value. Unexpectedly, the yield of picolinate produced in the mutant reaction is considerably lower (57%) than the quantitative conversion observed with the wild-type enzyme (Figure 3A, trace 4).

Inactivation of the mutant during turnover could prevent complete consumption of P2C, an event that would result in a low apparent yield of picolinate. To test this hypothesis, an aliquot of wild-type nikD was added to the spent mutant reaction

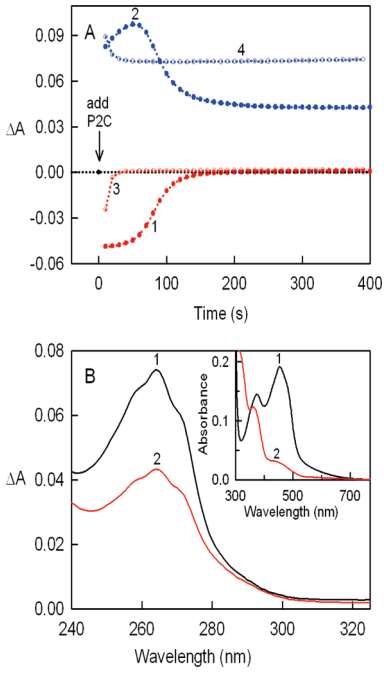

FIGURE 3: Enzyme-monitored turnover and picolinate formation during reaction of 5.1 μM wild-type nikD or 5.8 μM Tyr258Phe with 20 μM P2C in air-saturated 50 mM potassium phosphate buffer (pH 8.0) at 25 °C. The results are averages of duplicate reactions. (A) Absorbance changes observed at 456 nm after Tyr258Phe and wild-type nikD had been mixed with P2C are shown in curves 1 and 3, respectively. Changes in absorbance observed at 264 nm with the mutant and wild-type enzyme are shown in curves 2 and 4, respectively. (B) The UV absorption spectrum of the product formed in the reaction with wild-type nikD (curve 1) or Tyr258Phe (curve 2) was determined by subtracting the spectrum observed before substrate addition from that observed after the reaction was complete. The inset shows the anaerobic reduction of Tyr258Phe with P2C. Curve 1 is the absorption spectrum of the mutant (20 μM) in 100 mM potassium phosphate buffer (pH 8.0) containing 50 mM glucose and glucose oxidase (15 units/mL) at 25 °C. Curve 2 was recorded immediately after addition of 24 μM P2C. The original spectrum of the oxidized enzyme was restored upon aeration (spectrum not shown).

mixture. Formation of additional picolinate was not observed, indicating that all of the P2C had been consumed by the mutant. On the other hand, addition of a fresh aliquot of P2C to the spent mutant reaction mixture did initiate a second cycle of picolinate formation, similar to that observed for the first aliquot (data not shown). The results show that Tyr258Phe is not inactivated during turnover with P2C.

P2C is only moderately stable under assay conditions and also known to undergo decarboxylation in the presence of hydrogen peroxide (*29*). Turnover of the mutant with P2C is much slower than the corresponding reaction with wild-type nikD (see Figure 3A), suggesting that substrate decomposition might be a factor. Inclusion of excess catalase in the mutant reaction mixture did not affect the yield of picolinate, ruling out a peroxide-mediated decarboxylation of P2C. The yield of picolinate was also unaffected when the reaction with wild-type nikD was conducted using 10-fold less enzyme to mimic the slower rate observed with the mutant (data not shown). We conclude that substrate decomposition is not a relevant factor.

Mutation of Tyr258 Causes Partial Uncoupling of the Aromatization of P2C. 3,4-Dehydro-L-proline acts as an alternate substrate for nikD. The wild-type enzyme catalyzes the conversion of 3,4-dehydro-L-proline to pyrrole-2-carboxylate in an aromatization reaction that involves only a single redox cycle, unlike P2C (*8*, *9*). Significantly, turnover of Tyr258Phe (5 μM) with 3,4-dehydro-L-proline (20 μM) results in the quantitative formation of the expected two-electron oxidation product (data not shown). Importantly, anaerobic reaction of Tyr258Phe (20 μM) with a slight excess of P2C results in complete reduction of the mutant enzyme in a reaction that is fully reversible upon aeration (Figure 3B, inset). This outcome indicates that the mutant catalyzes the quantitative conversion of P2C to DHP under anaerobic conditions and strongly suggests that the same reaction occurs under aerobic conditions where oxygen will react with the reduced enzyme to produce 1 equiv of hydrogen peroxide, analogous to the observed two-electron oxidation of 3,4-dehydro-L-proline. This scenario is consistent with the absence of unreacted P2C in spent mutant reaction mixtures.

The results indicate that mutation of Tyr258 to Phe causes an apparent defect in the coupling of the two two-electron oxidation reactions required for conversion of P2C to picolinate. We postulate that turnover of the mutant enzyme with P2C is accompanied by significant release of the reactive DHP intermediate into solution, a counterproductive step that short-circuits the catalytic cycle and results in a low yield of picolinate. This model predicts that the product ratio, [hydrogen peroxide]/[picolinate], will be equal to $(100 + X)/X$, where X is the observed yield of picolinate. To test this hypothesis, we measured the amount of hydrogen peroxide and picolinate produced after reaction of the mutant with 20 μM P2C in buffer saturated with 100% oxygen. Values of 2.79 ± 0.03 and 2.4 ± 0.1 were obtained for the product ratio using Amplex Red and *o*-dianisidine, respectively, as the chromogenic substrate in a horseradish peroxidase-coupled assay. The observed values are in good agreement with a predicted value of 2.6 (Table 6). We also determined the product ratio in control studies with wild-type nikD using Amplex Red or *o*-dianisidine. The observed values (2.2 ± 0.1 or 1.87 ± 0.02, respectively) are in accord with a ratio of 2.0 predicted for a fully coupled aromatization reaction. The results obtained with wild-type nikD are also consistent with the 2-fold difference in initial rates observed for hydrogen peroxide and picolinate formation, unlike Tyr258Phe where the product ratio is higher than the observed ratio of initial rates. The reason for this apparent discrepancy is unclear.

Tyr258 is unlikely to participate directly in P2C or DHP oxidation, as judged by the location and orientation of the tyrosyl side chain in the open (see Figure 1) or closed (*10*) form of the enzyme·picolinate complex. Nevertheless, a conservative mutation at this position appears to promote release of the reactive DHP intermediate and causes a 10−50-fold decrease in steady-state kinetic parameters. In an effort to deconvolute the unexpected and substantial effects of the mutation on aerobic turnover, we probed various segments of the postulated catalytic cycle (see Scheme 3), as described in the following sections.

Does Mutation of Tyr258 Affect the Kinetics or Thermodynamics of Substrate or Product Binding?. 1-Cyclohexenoate (CHA) is a 1-deaza analogue of the enamine tautomer of P2C. Rate constants for formation and dissociation of the wild-type nikD·CHA complex are very similar to values obtained for the complex formed with P2C (*18*). Titration of Tyr258Phe with CHA results in a progressive loss of the long-wavelength absorption band and an increase in the intensity of the band at 456 nm, accompanied by an enhancement of its vibronic resolution (Figure 4A). The observed spectral perturbation is virtually

Table 6: Product Analysis after Reaction of Tyr258Phe with P2C at Various Oxygen Concentrations[a]

		[product] (μM)		[H_2O_2]/[picolinate]	
[O_2] (mM)	[P2C] (μM)	picolinate	H_2O_2	observed	predicted[b]
0.065	20	10.8 ± 0.8	ND[c]		
0.27	20	11.4 ± 0.04	ND[c]		
1.29	20	12.45 ± 0.07	34.7 ± 0.3[d]	2.79 ± 0.03[d]	2.61 ± 0.03
1.29	20	12.6 ± 0.6	30.4 ± 0.4[e]	2.4 ± 0.1[e]	2.6 ± 0.3

[a]Reactions were conducted with 4−6 μM Tyr258Phe in 100 mM potassium phosphate buffer (pH 8.0) at 25 °C and monitored as described in the legend of Figure 3. Upon completion of the reaction, the amount of picolinate was determined on the basis of the observed absorbance increase at 264 nm. Aliquots of horseradish peroxidase and a chromogenic substrate (*o*-dianisidine or Amplex Red, as indicated) were then added to the spent reaction mixture. The amount of hydrogen peroxide was determined on the basis of the absorbance change observed at 460 nm (*o*-dianisidine) or 563 nm (Amplex Red), analogous to that described in Experimental Procedures for initial rate measurements using a horseradish peroxidase-coupled assay. [b]Predicted values were estimated as described in the text. [c]Not determined. [d]Hydrogen peroxide determined using *o*-dianisidine. [e]Hydrogen peroxide determined using Amplex Red.

identical to that obtained with wild-type nikD, as judged by comparison of the corresponding difference spectra (Figure 4A, inset). The kinetics of formation of a complex with Tyr258Phe were determined by monitoring the monoexponential increase in absorption at 481 nm observed upon mixing the mutant with various concentrations of CHA in a stopped-flow spectrometer (Figure 4B). The observed rate constants exhibit a linear dependence on CHA concentration with a finite *y*-intercept (Figure 4B, inset), as expected for a simple one-step approach to equilibrium. Rate constants for complex formation (k_f) and dissociation (k_r) were obtained from the slope and intercept, respectively, of this plot. The kinetically determined dissociation constant ($K_d = k_r/k_f = 9 \pm 4$ μM) is, within experimental error, identical to a value determined by steady-state titration ($K_d = 8.6 \pm 0.2$ μM). The kinetic and thermodynamic parameters determined for the Tyr258Phe·CHA complex are very similar to values obtained with wild-type nikD (Table 7).

The spectral properties of the Tyr258Phe complex with picolinate closely resemble those obtained for the CHA complex (data not shown), as observed with wild-type nikD (*9*). Formation of the mutant picolinate complex is 2.9-fold slower and its dissociation 3.6-fold faster than observed with wild-type nikD, as judged by values obtained for the corresponding rate constants. The mutant complex is 5−10-fold less stable than the wild-type complex, as judged by values determined for its dissociation constant by steady-state titration or in kinetic studies (Table 7). The rate constant determined for dissociation of the Tyr258Phe·picolinate complex corresponds to the rate constant for the last step in the postulated minimal steady-state kinetic mechanism (k_6; see Scheme 3). Importantly, the observed value (k_r = 29.1 ± 0.6 s^{-1}) is more than 100-fold faster than turnover (k_{cat} = 0.26 ± 0.03 s^{-1}). The results indicate that product release is not rate-determining and cannot account for the 10-fold slower turnover rate observed with the mutant.

Does Mutation of Tyr258 Affect the Kinetics of Oxidation of P2C to DHP?. The rate of oxidation of P2C to DHP by Tyr258Phe was determined by using a stopped-flow spectrometer to monitor the reductive half-reaction under anaerobic conditions. An initial lag is observed at 456 nm when Tyr258Phe is mixed with 100 μM P2C, followed by a decrease in absorbance. The lag becomes progressively smaller as the P2C concentration

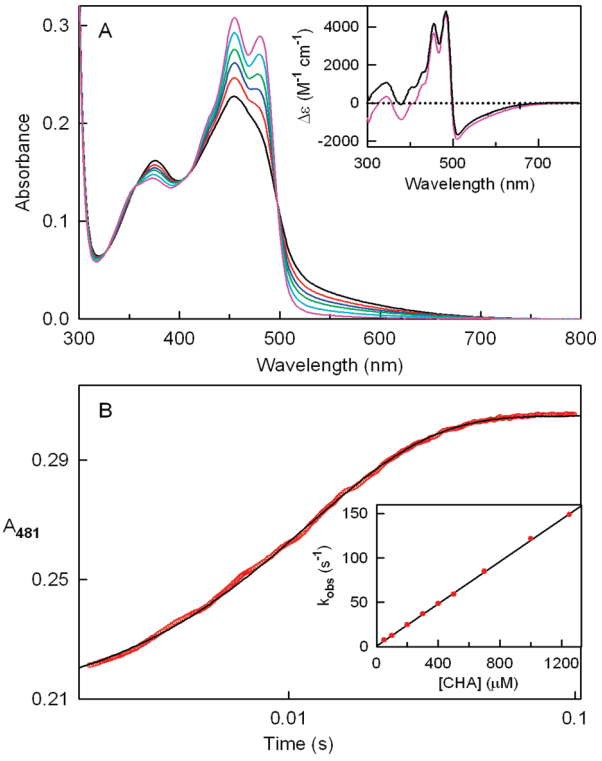

FIGURE 4: Steady-state titration (A) and kinetics of complex formation (B) observed with Tyr258Phe and CHA. Studies were conducted in 100 mM potassium phosphate buffer (pH 8.0) at 25 °C. (A) The black, red, blue, green, and cyan curves were recorded after addition of 0, 7.94, 15.75, 25.34, and 53.03 μM CHA, respectively. The magenta curve is the spectrum calculated for 100% complex formation, as detailed in Experimental Procedures. The inset compares difference spectra calculated for 100% CHA complex formation with Tyr258Phe (magenta curve) or wild-type nikD (black curve). The wild-type nikD difference spectrum was taken from ref *18*. (B) The red circles show the absorbance change observed with Tyr258Phe at 481 nm when the kinetics of complex formation with 700 μM CHA were monitored using a stopped-flow spectrometer in photomultiplier mode. The black line was obtained by fitting a single-exponential equation ($y = Ae^{-kt} + B$) to the data. The inset shows the effect of CHA concentration on the observed rate of complex formation. The black line was obtained by linear regression analysis of the data (red circles).

Table 7: Kinetics and Thermodynamics of Complex Formation with the Product or a Substrate Analogue[a]

	wild type[b]	Tyr258Phe
E_{ox}·CHA		
k_f (M^{-1} s^{-1})	(1.08 ± 0.02) × 10^5	(1.118 ± 0.008) × 10^5
k_r (s^{-1})	1.4 ± 0.1	1.0 ± 0.5
K_d (kinetic) (μM)	−	9 ± 4
K_d (static) (μM)	12.8 ± 0.9	8.6 ± 0.2
E_{ox}·picolinate		
k_f (M^{-1} s^{-1})	(2.83 ± 0.04) × 10^4	(0.97 ± 0.02) × 10^4
k_r (s^{-1})	8.0 ± 0.7	29.1 ± 0.6
K_d (kinetic) (μM)	280 ± 30	3000 ± 900
K_d (static) (μM)	290 ± 40	1300 ± 20

[a]Measurements were made in 100 mM potassium phosphate buffer (pH 8.0) at 25 °C. Values for K_d (static) were determined by steady-state titration. K_d (kinetic) = k_r/k_f. [b]Data for the picolinate and CHA complexes with wild-type nikD were taken from ref *18*. The value for k_r with picolinate was calculated using observed values for k_f and the K_d (static).

is increased and is not detectable in the reaction with 2500 μM P2C (Figure 5A). A similar lag is observed with wild-type nikD

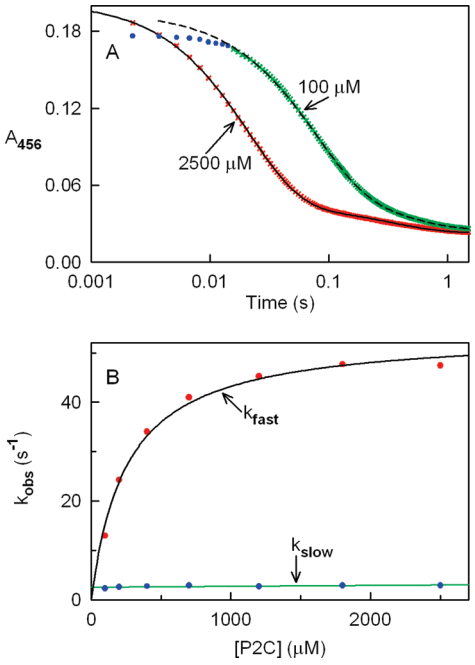

FIGURE 5: Kinetics of the anaerobic reduction of Tyr258Phe with P2C. Reactions were conducted in 100 mM potassium phosphate buffer (pH 8.0) at 25 °C and monitored using a stopped-flow spectrometer. Reaction traces at 456 nm were extracted from diode array data sets. (A) The solid black line was obtained by fitting a double-exponential equation ($y = Ae^{-k_{fast}t} + Be^{-k_{slow}t} + C$) to absorbance changes observed at 456 nm with 2500 μM P2C (red x's). The dashed black line was obtained by fitting a double-exponential equation to absorbance changes observed at 456 nm with 100 μM P2C (green x's), after data points had been excluded in the initial lag phase (blue circles), as previously described (*18*). (B) The solid black line was obtained by fitting a hyperbola [$k_{obs} = k_{lim}$ [P2C]/($K_{d,app}$ + [P2C])] to values obtained for k_{fast} (red circles) at different concentrations of P2C. The green line was obtained by linear regression analysis of values obtained for k_{slow} (blue circles) at different concentrations of P2C.

and has been shown to reflect a relatively slow formation of the enzyme·substrate complex (*18*).

The absorbance decrease at 456 nm observed with Tyr258Phe exhibits biexponential kinetics over a 25-fold range of P2C concentrations ($y = Ae^{-k_{fast}t} + Be^{-k_{slow}t} + C$). Most of the absorbance decrease occurs in a fast phase (88.3 ± 0.2%) and is attributed to the formation of a reduced enzyme·DHP complex. The observed rate constant of the fast phase exhibits a hyperbolic dependence on P2C concentration [$k_{obs} = k_{lim}$ [P2C]/($K_{d,app}$ + [P2C])] (Figure 5B), as observed with wild-type nikD (*18*). The limiting rate constant observed with Tyr258Phe at a saturating level of P2C (k_{lim} = 54 ± 1 s^{-1}) is ~200-fold faster than the observed turnover rate (k_{cat} = 0.26 ± 0.03 s^{-1}) and clearly not rate-determining. The value obtained for k_{lim} with the mutant is, within experimental error, identical to the limiting rate constant observed with wild-type nikD (k_{lim} = 53 ± 1 s^{-1}) (*18*). The results indicate that the mutation does not affect the rate of oxidation of P2C to DHP.

Studies with wild-type nikD show that P2C is a sticky substrate (*18*). For a sticky substrate, $K_{d,app}$ is equal to the ratio (k_r + k_{lim})/k_f, where k_f and k_r are rate constants for formation and dissociation of the ES complex, respectively. Tyr258Phe and wild-type nikD exhibit identical values of $K_{d,app}$ (Table 4). The results indicate that the mutation is unlikely to affect the kinetics of substrate binding, similar to results obtained with CHA, a P2C analogue (see Table 7).

The ratio $k_{lim}/K_{d,app}$ corresponds to the apparent second-order rate constant for the reaction of oxidized enzyme with P2C [$k_{lim}/K_{d,app} = k_f k_{lim}/(k_r + k_{lim})$] and should be equal to the ratio $k_{cat}/K_{m,P2C}$ for the steady-state mechanism shown in Scheme 3 [$k_{cat}/K_{m,P2C} = k_1k_2/(k_{-1} + k_2)$]. For wild-type nikD, identical values are obtained for this parameter using reductive half-reaction or steady-state kinetic parameters (Table 4). In sharp contrast, a major discrepancy is found with the mutant enzyme where the value calculated using reductive half-reaction parameters [$k_{lim}/K_{d,app} = (2.2 \pm 0.2) \times 10^5$ M^{-1} s^{-1}] is 60-fold larger than the value obtained using steady-state kinetic parameters [$k_{cat}/K_{m,P2C} = (3.7 \pm 0.7) \times 10^3$ M^{-1} s^{-1}]. The basis for this disparity will be discussed.

The rate constant observed for the slow phase of the reductive half-reaction with Tyr258Phe is independent of the concentration of P2C (k_{slow} = 2.78 ± 0.08 s^{-1}) (Figure 5B), 10-fold faster than the rate of turnover (k_{cat} = 0.26 ± 0.03 s^{-1}), and, within experimental error, identical to the rate constant obtained for the slow phase with the wild-type enzyme (k_{slow} = 2.7 ± 0.1 s^{-1}). The slow step appears to be rate-determining during turnover of wild-type nikD (k_{cat} = 2.3 ± 0.2 s^{-1}) and is thought to involve isomerization of the reduced enzyme·DHP complex, as judged by results obtained in studies with deuterium-labeled P2C (*18*). Unlike the case with wild-type nikD, the slow step may, at best, be only partially rate-determining with Tyr258Phe and certainly cannot account for the 10-fold slower turnover rate observed with the mutant enzyme.

Spectral Course of the Anaerobic Reduction of Tyr258Phe with P2C. Formation of the ES complex with wild-type nikD results in an increase in absorption at 456 nm and partially overlaps with the onset of enzyme reduction, features that give rise to the initial lag observed when enzyme reduction is monitored at this wavelength (*18*). A similar ES complex is formed with Tyr258Phe, as judged by the isosbestic set of spectra recorded immediately (t = 0.74 ms) after the mutant was mixed with various concentrations of P2C (Figure 6A). The mutant ES complex exhibits enhanced absorption in the 456 nm region and a broad increase in absorption in the long-wavelength region (λ > 570 nm), similar to the wild-type complex. The new long-wavelength absorption band is attributed to charge-transfer interaction between FAD and the electron-rich enamine tautomer of P2C, as proposed for the wild-type ES complex (*18*).

The spectral course observed during the fast phase of Tyr258Phe reduction with 100 μM P2C (Figure 6B, curves 1−10) exhibits an isosbestic point at 350 nm that is lost during the slow phase of the reaction (Figure 6B, curves 11 and 12). The final spectrum observed for reduced Tyr258Phe exhibits a fairly sharp maximum at 361 nm that is bathochromically shifted as compared with the broader peak observed for the corresponding species formed with wild-type nikD (λ_{max} = 355 nm) (Figure 6B, inset). The spectral course of the mutant reaction is similar to that observed with wild-type nikD, except that loss of the isosbestic point is hardly detectable during the slow phase of the wild-type enzyme reaction. This difference may be related to the difference noted above in the spectral properties of the final reduced species formed with the mutant and wild-type enzyme. A very small transient increase in absorption in the long-wavelength region (λ > 535 nm) can be detected during reduction of Tyr258Phe with 100 μM P2C, as observed with wild-type nikD (*18*). The magnitude and complexity of the absorbance changes in the long-wavelength region are more pronounced at higher P2C concentrations, which can be seen in the spectral course observed for the

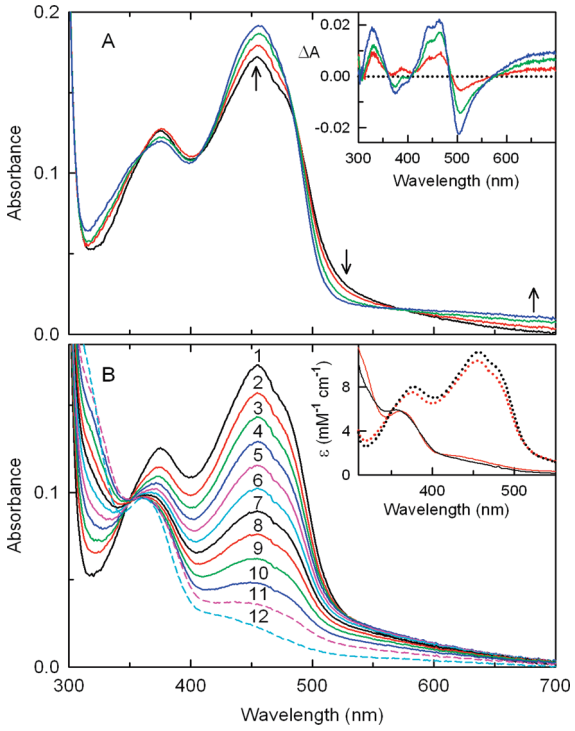

FIGURE 6: Formation of an initial enzyme·substrate complex (A) and spectral course of the anaerobic reduction of Tyr258Phe with 100 μM P2C (B). Reactions were conducted in 100 mM potassium phosphate buffer (pH 8.0) at 25 °C and monitored using a stopped-flow diode array data spectrometer. (A) Absorption spectra recorded 0.74 ms after Tyr258Phe was mixed with 0, 400, 1200, and 2500 μM P2C are shown as black, red, green, and blue curves, respectively. Arrows indicate the direction of spectral changes observed as the concentration of P2C is increased. The inset shows the corresponding difference spectra obtained by subtracting the spectrum of free Tyr258Phe from spectra observed in the presence of P2C. (B) Spectra were recorded from 0.74 ms (curve 1) to 7.125 s (curve 12) after Tyr258Phe was mixed with 100 μM P2C. Curves 2−11 were recorded 20.2, 30.7, 42.7, 55.5, 70.5, 88.5, 112.5, 150.0, 216.0, and 363.0 ms, respectively, after mixing. The inset compares initial (t = 0.74 ms) (dotted lines) and final (t = 7.125 s) (solid lines) absorption spectra observed after reaction of Tyr258Phe (red lines) or wild-type nikD (black lines) with 100 μM P2C. The wild-type nikD data were taken from ref *18*.

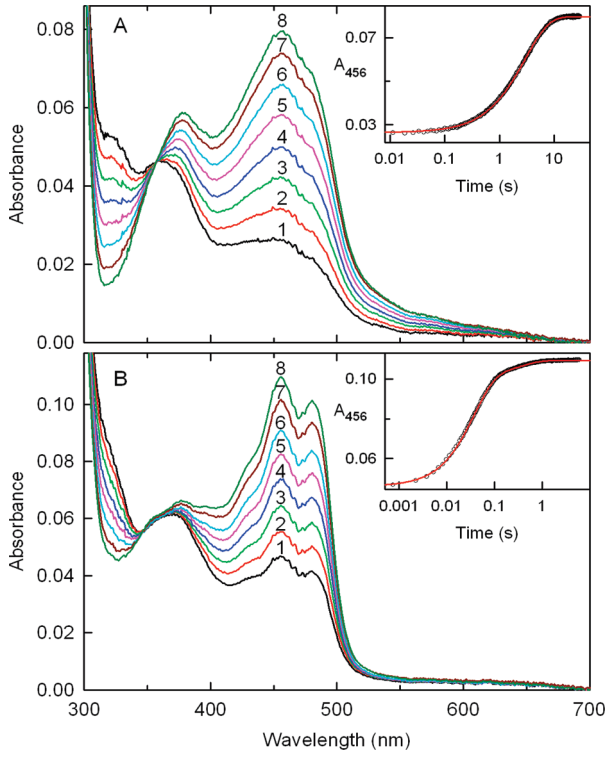

FIGURE 7: Oxidation of reduced wild-type nikD by reaction with molecular oxygen (0.65 mM) as monitored by diode array stopped-flow spectometry. Reactions were conducted in 100 mM potassium phosphate buffer (pH 8.0) at 25 °C in the absence (A) or presence (B) of 12 mM CHA. The reduced enzyme was prepared by reaction with a stoichiometric amount of 3,4-dehydro-L-proline, as detailed in Experimental Procedures. (A) Curves 1−8 were recorded 3.74×10^{-3}, 0.4425, 0.9900, 1.6800, 2.6550, 4.0050, 6.7650, and 29.9250 s, respectively, after the anaerobic reduced enzyme was mixed with aerobic buffer. The inset shows a plot of the observed absorption increase at 456 nm. The red line was obtained by fitting an equation for a single-exponential rise [$y = A(1 - e^{-kt}) + B$] to the data (●). (B) Curves 1−8 were recorded 0.74, 6.74, 14.2, 24.7, 38.2, 58.5, 124.5, and 7,125 ms, respectively, after the anaerobic reduced enzyme was mixed with aerobic buffer. The inset shows a plot of the observed absorption increase at 456 nm. The red line was obtained by a fitting an equation for a double-exponential rise [$y = A(1 - e^{-k_1 t}) + B(1 - e^{-k_2 t}) + C$] to the data (●).

reaction of Tyr258Phe with 2500 μM P2C (see Figure S2 of the Supporting Information). A similar feature is seen with wild-type nikD (*18*).

Identification of Factors That Affect Activation of Oxygen by Reduced NikD. NikD oxidizes 3,4-dehydro-L-proline to pyrrole-2-carboxylate, a compound that forms a relatively unstable complex with the oxidized enzyme (K_d = 0.46 mM) (*8*, *9*). Ligand-free reduced wild-type or mutant enzyme was prepared by anaerobic reaction with 1 equiv of 3,4-dehydro-L-proline. The oxidative half-reaction was monitored by mixing reduced wild-type or mutant nikD with aerobic buffer in a stopped-flow spectrophotometer. In each case, an isosbestic conversion of the reduced enzyme to the corresponding oxidized species is observed (Figures 7A and 8A). It is noteworthy that both reactions are much slower than those observed with other flavoprotein oxidases and can even be monitored using a steady-state diode array spectrometer (data not shown). Rate constants were determined by fitting a single-exponential equation to the observed increase in absorbance at 456 nm (see the insets in Figures 7A and 8A). Values observed at different oxygen concentrations with the wild-type or mutant enzyme are directly proportional to the oxygen concentration (Figure 9).

The second-order rate constant obtained for the reaction of free reduced wild-type nikD with oxygen (k = 530 ± 20 M^{-1} s^{-1}) is only 2-fold larger than the value reported for free reduced flavin (Table 8). Indeed, the rate constant observed with nikD is at least 1 order of magnitude smaller than values obtained with other free reduced flavoprotein oxidases, including enzymes that exhibit a ternary complex steady-state kinetic mechanism (*30*). To evaluate the kinetic competence of free reduced wild-type nikD, pseudo-first-order rate constants were calculated for the oxidative half-reaction at several finite oxygen concentrations (k_{calc}) and compared with values estimated for the apparent turnover rate ($k_{cat,app}$) at the same oxygen concentrations in the presence of a saturating level of P2C. For a kinetically competent intermediate, the ratio $k_{calc}/k_{cat,app}$ should be ≥1. However, values less than unity are obtained for this ratio over a 10-fold range of oxygen concentrations [$k_{calc}/k_{cat,app}$ = 0.19 ± 0.02 (0.129 mM O_2) or 0.43 ± 0.03 (1.29 mM O_2)]. The results rule out the free reduced enzyme as a catalytically significant intermediate during turnover of wild-type nikD.

Oxidation of free reduced Tyr258Phe (k = 153 ± 1 M^{-1} s^{-1}) is 3.5-fold slower than that of wild-type nikD and even slower than

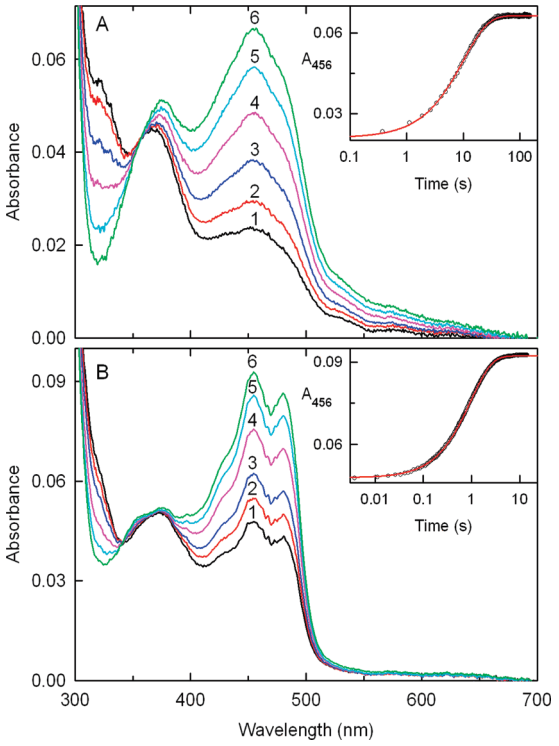

FIGURE 8: Oxidation of reduced Tyr258Phe by reaction with molecular oxygen (0.65 mM) as monitored by diode array stopped-flow spectrometry. Reactions were conducted in 100 mM potassium phosphate buffer (pH 8.0) at 25 °C in the absence (A) or presence (B) of 12 mM CHA. The reduced enzyme was prepared by reaction with a stoichiometric amount of 3,4-dehydro-L-proline, as detailed in Experimental Procedures. (A) Curves 1−6 were recorded 0.375, 1.875, 4.875, 9.375, 16.875, and 49.125 s, respectively, after the anaerobic reduced enzyme was mixed with aerobic buffer. (B) Curves 1−6 were recorded 3.74×10^{-3}, 0.1612, 0.3675, 0.9300, 1.8750, and 14.250 s, respectively, after the anaerobic reduced enzyme was mixed with aerobic buffer. The inset in each panel shows a plot of the observed absorption increase at 456 nm. The red line in each inset was obtained by fitting an equation for a single-exponential rise [$y = A(1 - e^{-kt}) + B$] to the data (●).

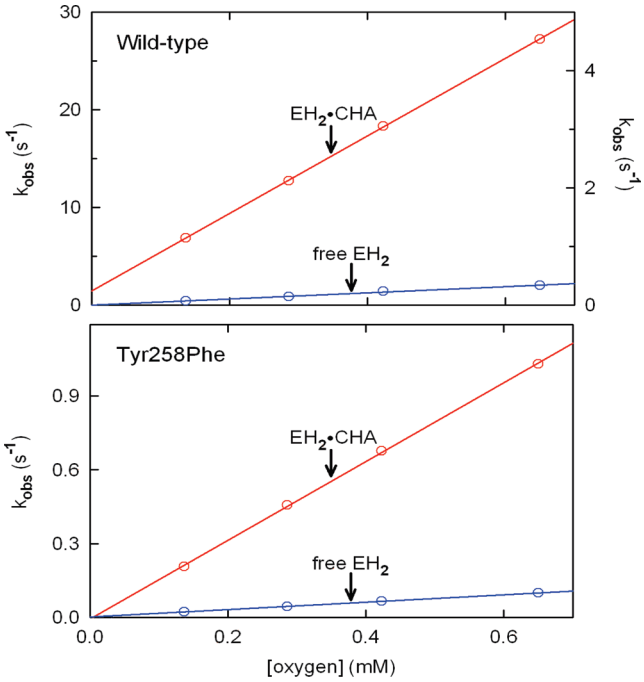

FIGURE 9: Effect of oxygen concentration on the observed rate of oxidation of reduced wild-type nikD (top) or reduced Tyr258Phe (bottom). Reactions were conducted at different oxygen concentrations in the presence (red circles) or absence (blue circles) of 12 mM CHA, as described in the legends of Figures 7 and 8. The solid lines were generated by linear regression analysis of the data. For wild-type nikD (top panel), values for k_{obs} in the absence CHA are plotted according to the right-hand axis; the observed rate constant of the fast phase in the presence of CHA is plotted according to the left-hand axis.

the reaction observed with free reduced flavin (Table 8). Nevertheless, it is not possible to rule out the free reduced enzyme as an intermediate during turnover of the mutant, as judged by the criterion described above [$k_{obs}/k_{cat,app} = 1.4 \pm 0.3$ (0.129 mM O_2) or 2.0 ± 0.4 (1.29 mM O_2)].

Steady-state kinetic studies with wild-type nikD or Tyr258Phe are consistent with a mechanism in which oxygen reacts with a reduced enzyme·DHP complex (see Scheme 3). As a model for this step, we monitored the reaction of oxygen with reduced enzyme·CHA complexes formed with wild-type or mutant nikD. In each case, an isosbestic conversion of the reduced complex to the corresponding oxidized complex is observed, as judged by the characteristic, highly resolved, absorption band seen for the oxidized sample at 456 nm (Figures 7B and 8B).

Oxidation of the reduced wild-type nikD·CHA complex exhibits biphasic kinetics in which most of the observed spectral change (81 ± 3%) occurs in an initial fast phase (Figure 7B, inset). The observed rate constant of the fast phase is directly proportional to the concentration of oxygen (Figure 9, top panel). The second-order rate constant obtained for the fast phase [$k = (3.97 \pm 0.03) \times 10^4$ M^{-1} s^{-1}] is 75-fold larger than that observed for the free reduced wild-type enzyme (Table 8) and within the range of values observed with other flavoprotein oxidases (*30*). The slow phase is independent of oxygen concentration ($k_{slow} = 2.6 \pm 0.2$ s^{-1}). The nature of this phase is unclear. A similar oxygen-independent slow phase (5−10 s^{-1}) is observed with cholesterol oxidase (*31*) and an oxidase-like mutant of galactonolactone dehydrogenase (*32*). Unlike those for CHA, monophasic kinetics are observed for the oxidation of a complex of reduced wild-type nikD with benzoate or picolinate (data not shown). The second-order rate constants obtained for the oxidation of these complexes are ~10-fold greater than that observed with the ligand-free reduced enzyme (Table 8). The reduced enzyme·picolinate complex is kinetically competent, as judged by values obtained for the ratio

Table 8: Rate Constants for the Oxidation of Reduced Wild-Type NikD or Tyr258Phe by Molecular Oxygen[a]

	k_{obs} (M^{-1} s^{-1})		
reduced species	wild type	Tyr258Phe	free flavin[b]
(E)-$FADH_2$	530 ± 20 (540 ± 40)[c]	153 ± 1	250
E-$FADH_2$·CHA	(3.97 ± 0.03) × 10^4[d]	(1.60 ± 0.02) × 10^3	
E-$FADH_2$·benzoate	(5.0 ± 0.1) × 10^3		
E-$FADH_2$·picolinate	(4.1 ± 0.2) × 10^3		

[a]Unless otherwise indicated, reactions were conducted at 25 °C in 100 mM potassium phosphate (pH 8.0) in the absence or the presence of 12 mM CHA, benzoate, or picolinate and monitored by following the increase in absorbance at 456 nm. Except as noted, reactions were monitored using a stopped-flow spectrometer in diode array mode and exhibited monophasic kinetics. [b]Data previously reported (*33*). [c]The reaction was conducted at 25 °C in 100 mM tetramethylammonium phosphate (pH 8.0) and monitored using a steady-state diode array spectrometer. [d]The reaction exhibited biphasic kinetics, as discussed in the text. The table lists the bimolecular rate constant for the initial fast phase. The slow phase is independent of oxygen concentration ($k_{slow} = 2.6 \pm 0.2$ s^{-1}).

$k_{calc}/k_{cat,app}$ [1.5 ± 0.2 (0.129 mM O_2) or 3.3 ± 0.3 (1.29 mM O_2)], consistent with the mechanism proposed in Scheme 3.

Monophasic kinetics are observed for the reaction of oxygen with the reduced Tyr258Phe·CHA complex (Figure 8B, inset). Rate constants observed at different oxygen concentrations are directly proportional to the oxygen concentration (Figure 9, bottom panel). The second-order rate constant obtained for the reaction of oxygen with the reduced mutant·CHA complex [$k = (1.60 \pm 0.02) \times 10^3$ M^{-1}] is 10-fold faster than that observed for the reaction with ligand-free reduced Tyr258Phe (Table 8). However, oxidation of the reduced Tyr258Phe·CHA complex is 25-fold slower than the reaction with the corresponding wild-type complex. A similar effect of the mutation on oxygen reactivity is also observed during turnover, as estimated by the 20-fold decrease in the value obtained for $k_{cat}/K_{m,oxygen}$ (Table 4).

A slower rate of oxidation of the catalytically significant reduced Tyr258Phe·DHP complex might allow release of the reactive intermediate into solution during turnover, short-circuiting the normal catalytic cycle. We reasoned that dissociation of the complex might be thwarted by increasing the rate of complex oxidation. The rate of complex oxidation should be directly proportional to the oxygen concentration, as judged by results obtained for the reduced Tyr258Phe·CHA complex. This scenario predicts that turnover of Tyr258Phe with P2C at higher concentrations of oxygen should result in a corresponding increase in the yield of picolinate. However, a 20-fold increase in oxygen concentration (from 0.065 to 1.29 mM) caused only a small increase (from 54 to 63%) in the observed yield of picolinate (Table 6). The results indicate that the reduced oxygen reactivity of the mutant cannot account for the observed partial uncoupling of the aromatization reaction.

DISCUSSION

Mutation of Tyr258 to Phe does not perturb the structure of nikD but does cause a 10-fold decrease in the turnover rate observed at saturating P2C and oxygen concentrations. The mutation does not affect the rate of ligand binding or dissociation, as judged by results obtained with P2C or CHA, whereas a modest difference (<4-fold) is observed with picolinate. Tyr258Phe catalyzes a quantitative two-electron oxidation of P2C, but only 60% of the DHP intermediate formed in this reaction undergoes a second redox cycle to produce picolinate. The mutation does not affect the stoichiometry of the reaction observed with 3,4-dehydro-L-proline, an alternate substrate that is converted to an aromatic product in a single two-electron oxidation step. Wild-type and mutant enzymes exhibit identical rates for the oxidation P2C to DHP, suggesting that a similar outcome is likely for the more favorable oxidation of DHP to picolinate. The rate of oxidation of P2C to DHP by the mutant is 200-fold faster than its rate of turnover. The rate of isomerization of the reduced enzyme·DHP complex is unaffected by mutation of Tyr258. The rate of isomerization is equal to the turnover rate observed with wild-type nikD but 10-fold faster than the mutant turnover rate. Dissociation of the Tyr258Phe·picolinate complex is more than 100-fold faster than the mutant turnover rate. The results indicate that the 10-fold decrease in the turnover rate observed with Tyr258Phe is unlikely to be caused by a decrease in the rate constant of any of the unimolecular steps in the postulated minimal steady-state kinetic mechanism (see Scheme 3). However, the currently unknown kinetic mechanism for oxidation of DHP to picolinate may be more complex than shown in Scheme 3. For example, the indicated redox step may be preceded by a conformational change in the oxidized enzyme·DHP complex that might be 10-fold slower with the mutant enzyme, as discussed below.

The results show that mutation of Tyr258 causes a defect in the coupling of the two two-electron oxidation reactions required for the conversion of P2C to picolinate. The observed uncoupling is attributed to release of the reactive DHP intermediate from a catalytic complex. The mutation may promote complex dissociation by decreasing the rate of the next step in the catalytic reaction. For example, a decrease in the rate of the reaction with oxygen might favor release of the intermediate from the reduced enzyme·DHP complex. Although the mutant does exhibit reduced oxygen reactivity, a 20-fold increase in oxygen concentration does not result in an appreciable increase in the yield of picolinate observed during turnover. This outcome argues against dissociation of the reduced enzyme·DHP complex. Further evidence is provided by the observed intersecting line double-reciprocal plots because dissociation of a reduced enzyme·DHP complex would introduce an irreversible step prior to reaction of the reduced enzyme with oxygen, a scenario expected to yield parallel line double-reciprocal plots. The results strongly suggest that the intermediate is released from an oxidized enzyme·DHP complex. As indicated in Scheme 2, formation of picolinate may involve oxidation of one of two possible DHP isomers. It is noteworthy that oxidation of DHP isomer C requires a 180° flip of the intermediate and transient formation of an "open complex". This conformational change requires movement of Tyr258 and other residues that comprise the "aromatic cage", as judged by crystal structures of the open and closed forms of the oxidized enzyme·picolinate complex (*10*). Mutation of Tyr258 might somehow increase the lifetime of the "open complex" and thus promote release of the reactive DHP intermediate into solution. The fate of the released intermediate is unknown and a subject for future studies.

The postulated dissociation of the oxidized enzyme·DHP complex introduces a branch in the proposed minimal steady-state kinetic mechanism (see Scheme 3) and results in a complicated rate equation that contains squared terms in oxygen concentration in both the numerator and denominator.[2] The complexity expected for a branched mechanism is not apparent in the steady-state kinetic data obtained for Tyr258Phe within the accessible range of oxygen concentrations, as judged by the linear double-reciprocal plots and the good fit ($R^2 = 0.9881$) to the data obtained using an equation (eq 1) for an unbranched sequential mechanism. However, the apparent second-order rate constant for the reaction of the mutant with P2C, estimated on the basis of steady-state kinetic parameters ($k_{cat}/K_{m,P2C}$), does not match a value determined on the basis of reductive half-reaction parameters ($k_{lim}/K_{d,app}$). The observed 60-fold discrepancy rules out a simple sequential mechanism but is consistent with the postulated branched mechanism. Importantly, the agreement between steady-state and reductive half-reaction kinetic parameters, predicted for a simple sequential mechanism, is observed with wild-type nikD (*18*) and other mutants (*17*) that exhibit quantitative coupling of the two redox cycles required for conversion of P2C to picolinate.

The previously unknown parameters that affect activation of oxygen by wild-type nikD were investigated in conjunction with

[2]The rate equation for the branched mechanism was derived using WinSites (*1*).

studies to evaluate the effect of the Tyr258Phe mutation on every accessible segment of the catalytic cycle. The results rule out the ligand-free reduced enzyme as a kinetically competent intermediate during turnover of wild-type nikD, consistent with the proposed sequential mechanism (see Scheme 3). In fact, the rate of reaction of ligand-free reduced nikD with oxygen ($k = 530 \pm 20$ M^{-1} s^{-1}) is nearly as slow as that observed with free reduced flavin ($k = 250\ M^{-1}\ s^{-1}$) and at least 1 order of magnitude slower than that observed with other ligand-free reduced flavoprotein oxidases, including MSOX [$k = (2.83 \pm 0.07) \times 10^5\ M^{-1}\ s^{-1}$] (*19*, *30*). The 500-fold difference in rates observed with nikD and MSOX is not surprising, given that the single basic residue responsible for oxygen activation by MSOX (Lys265) is not conserved in nikD. Although MSOX is the closest nikD structural homologue (root-mean-square deviation of 1.38 Å), a mobile loop that binds K^+ or Na^+ ions is found only in nikD (*10*). The reaction of ligand-free reduced nikD with oxygen is unaffected when K^+ in the standard reaction buffer is replaced with a much larger counterion [$(CH_3)_4N^+$] that cannot fit into the cation-binding loop (see Table 8). The results indicate that this loop is unlikely to play a role in the activation of oxygen by nikD. Unlike MSOX, the presence of bound substrate or product appears to be a key factor in the activation of oxygen by nikD, as judged by the 10−75-fold faster rates observed for complexes of the reduced enzyme with picolinate, benzoate, or CHA. The results also show that the reduced enzyme·picolinate complex is kinetically competent, consistent with the proposed minimal steady-state kinetic mechanism (see Scheme 3). A ligand-induced rate acceleration is observed with reduced Tyr258Phe, but the mutant complex is 25-fold less reactive with oxygen compared with wild-type nikD, as judged by results obtained with CHA.

The rate-determining step in the reaction of reduced flavins with oxygen involves transfer of an electron to produce a flavin/superoxide anion radical pair (*30*, *33*−*36*). The rate accelerations observed upon binding of anionic ligands[3] to reduced nikD must, therefore, be achieved by decreasing the activation energy for the initial one-electron transfer step. The presence of a nearby negative charge may decrease the reduction potential of the flavin and thus increase the driving force of the reaction by making the flavin a more potent reductant. However, the active site, at least in oxidized enzyme complexes, appears to be less polar than ligand-free enzyme, as judged by the presence of a highly resolved 456 nm absorption band. A more hydrophobic active site is expected to decrease the potential of the oxygen−superoxide couple, exerting a negative effect on the driving force of the reaction. However, it may not be appropriate to assume that properties observed for complexes with oxidized nikD can be extrapolated to those formed with the reduced enzyme. For example, solution studies indicate that the ligand in oxidized complexes is stacked atop the flavin ring, as judged by the absence of an FAD−Trp355 charge-transfer band (*9*, *20*). NikD is known to exhibit two distinct ligand binding modes, a feature that allows for the possibility that an alternate mode may be favored in the reduced enzyme. Ligand-induced rate accelerations have been reported for other flavoprotein oxidases where the observed effect is typically attributed to the presence of a positively charged group in the ligand (*30*, *37*). The mechanism of the anion-induced rate acceleration observed with nikD is unclear and a subject for future investigation.

Concluding Remarks. NikD catalyzes a remarkable aromatization reaction comprising two redox cycles and at least one isomerization step. In the wild-type enzyme, the multistep catalytic process is orchestrated by a finely tuned active site that sequesters reactive intermediates and synchronizes activation of oxygen to the formation of reduced enzyme complexes with a redox intermediate or the final aromatic product. This efficient coupling of redox cycles and synchronization of oxygen activation is disrupted by apparently subtle changes in active site dynamics induced upon mutation of Tyr258, a residue that forms part of an "aromatic cage" that surrounds the ring in picolinate and its precursors. Results obtained with nikD may provide a paradigm for related reactions in which detailed mechanistic studies are less feasible because the substrates are not small molecules. For example, the aromatization of L-prolyl residues covalently tethered to a peptidyl carrier protein is mediated by flavoenzymes in reactions that produce the pyrrole-2-carboxyl units that are required for the nonribosomal biosynthesis of various peptide antibiotics (e.g., chlorobiocin and pyoluteorin) (*38*, *39*).

SUPPORTING INFORMATION AVAILABLE

Steady-state kinetic analysis of P2C oxidation by Tyr258Phe (Figure S1) and spectral course of the anaerobic reduction of Tyr258Phe with 2500 μM P2C (Figure S2). This material is available free of charge via the Internet at http://pubs.acs.org.

REFERENCES

1. Yago, J. M., Sevilla, F. G., Garrido del Solo, C., Duggleby, R. G., and Varon, R. (2006) A Windows program for the derivation of steady-state equations in enzyme systems. *Appl. Math. Comput. 181*, 837–852.
2. Lauer, B., Russwurm, R., Schwarz, W., Kalmanczhelyi, A., Bruntner, C., Rosemeier, A., and Bormann, C. (2001) Molecular characterization of co-transcribed genes from *Streptomyces tendae Tu901* involved in the biosynthesis of the peptidyl moiety and assembly of the peptidyl nucleoside antibiotic nikkomycin. *Mol. Gen. Genet. 264*, 662–673.
3. Hector, R. F. (1993) Compounds active against cell walls of medically important fungi. *Clin. Microb. Rev. 6*, 1–21.
4. Bruntner, C., and Bormann, C. (1998) The *Streptomyces tendae Tu901* L-lysine 2-aminotransferase catalyzes the initial reaction in nikkomycin D biosynthesis. *Eur. J. Biochem. 254*, 347–355.
5. Macholan, L., and Svatek, E. (1960) Aminoketocarbonsauren VL: Über die konstitution and strukturformen der α-keto-analoga natürlichler diaminosäuren. *Collect. Czech. Chem. Commun. 25*, 2564–2575.
6. Srinivasan, R., and Fisher, H. F. (1986) Structural features facilitating the glutamate dehydrogenase catalyzed α-imino acid-α-amino acid interconversion. *Arch. Biochem. Biophys. 246*, 743–750.
7. Jorns, M. S., Bruckner, R. C., Zhao, G., Carrell, C. J., and Mathews, F. S. (2005) NikD: Crystal structures, charge transfer complex and endogenous ligands. In Flavins and Flavoproteins 2005 (Nishino, T., Miura, R., Tanokura, M., and Fukui, K., Eds.) pp 773−785, ARchiTech Inc., Tokyo.
8. Bruckner, R. C., Zhao, G., Venci, D., and Jorns, M. S. (2004) Nikkomycin biosynthesis: Formation of a 4-electron oxidation product during turnover of nikD with its physiological substrate. *Biochemistry 43*, 9160–9167.
9. Venci, D., Zhao, G., and Jorns, M. S. (2002) Molecular characterization of nikD, a new flavoenzyme important in the biosynthesis of nikkomycin antibiotics. *Biochemistry 41*, 15795–15802.
10. Carrell, C. J., Bruckner, R. C., Venci, D., Zhao, G., Jorns, M. S., and Mathews, F. S. (2007) NikD, an unusual amino acid oxidase essential for nikkomycin biosynthesis: Structures of closed and open forms at 1.15 and 1.90 Å resolution. *Structure 15*, 928–941.
11. Khanna, P., and Jorns, M. S. (2001) Characterization of the FAD-containing N-methyltryptophan oxidase from *Escherichia coli*. *Biochemistry 40*, 1441–1450.

[3]Recent studies indicate that nikD binds the anionic rather than the zwitterionic form of picolinate (R. C. Bruckner and M. S. Jorns, unpublished results).

12. Wu, X. L., Takahashi, M., Chen, S. G., and Monnier, V. M. (2000) Cloning of amadoriase I isoenzyme from *Aspergillus sp.*: Evidence of FAD covalently linked to Cys342. *Biochemistry 39*, 1515–1521.
13. Miura, S., Ferri, S., Tsugawa, W., Kiin, S., and Sode, K. (2006) Active site analysis of fructosyl amine oxidase using homology modeling and site-directed mutagenesis. *Biotechnol. Lett. 28*, 1895–1900.
14. Dodt, G., Kim, D. G., Reimann, S. A., Reuber, B. E., McCabe, K., Gould, S. J., and Mihalik, S. J. (2000) L-Pipecolic acid oxidase, a human enzyme essential for the degradation of L-pipecolic acid, is most similar to the monomeric sarcosine oxidases. *Biochem. J. 345*, 487–494.
15. Wagner, M. A., Khanna, P., and Jorns, M. S. (1999) Structure of the flavocoenzyme of two homologous amine oxidases: Monomeric sarcosine oxidase and N-methyltryptophan oxidase. *Biochemistry 38*, 5588–5595.
16. Trickey, P., Wagner, M. A., Jorns, M. S., and Mathews, F. S. (1999) Monomeric sarcosine oxidase: Structure of a covalently-flavinylated secondary amine oxidizing enzyme. *Structure 7*, 331–345.
17. Kommoju, P. R., Bruckner, R. C., Ferreira, P., and Jorns, M. S. (2009) Probing the role of active site residues in nikD, an unusual amino acid oxidase that catalyzes an aromatization reaction important in nikkomycin biosynthesis. *Biochemistry 48*, 6951–6962.
18. Bruckner, R. C., and Jorns, M. S. (2009) Spectral and kinetic characterization of intermediates in the aromatization reaction catalyzed by nikD, an unusual amino acid oxidase. *Biochemistry 48*, 4455–4465.
19. Zhao, G., Bruckner, R. C., and Jorns, M. S. (2008) Identification of the oxygen activation site in monomeric sarcosine oxidase: Role of Lys265 in catalysis. *Biochemistry 47*, 9124–9135.
20. Bruckner, R. C., Zhao, G., Ferreira, P., and Jorns, M. S. (2007) A mobile tryptophan is the intrinsic charge transfer donor in a flavoenzyme essential for nikkomycin antibiotic biosynthesis. *Biochemistry 46*, 819–827.
21. Ho, S. N., Hunt, H. D., Horton, R. M., Pullen, J. K., and Pease, L. R. (1989) Site-directed mutagenesis by overlap extension using the polymerase chain reaction. *Gene 77*, 51–59.
22. McPherson, A. (1999) Crystallization of biological macromolecules, Cold Spring Harbor Laboratory Press, Plainview, NY.
23. Otwinowski, Z., and Minor, W. (1997) Processing of X-ray diffraction data collected in oscillation mode. *Methods Enzymol. 276*, 307–326.
24. Mcree, D. E. (1999) Xtalview/xfit: A versatile program for manipulating atomic coordinates and electron density. *J. Struct. Biol. 125*, 156–165.
25. Wagner, M. A., and Jorns, M. S. (2000) Monomeric sarcosine oxidase: 2. Kinetic studies with sarcosine, alternate substrates and substrate analogs. *Biochemistry 39*, 8825–8829.
26. Hassan-Abdallah, A., Bruckner, R. C., Zhao, G., and Jorns, M. S. (2005) Biosynthesis of covalently bound flavin: Isolation and *in vitro* flavinylation of the monomeric sarcosine oxidase apoprotein. *Biochemistry 44*, 6452–6462.
27. Wagner, M. A., Trickey, P., Chen, Z., Mathews, F. S., and Jorns, M. S. (2000) Monomeric sarcosine oxidase: 1. Flavin reactivity and active site binding determinants. *Biochemistry 39*, 8813–8824.
28. Zhao, G., and Jorns, M. S. (2006) Spectral and kinetic characterization of the Michaelis charge transfer complex in monomeric sarcosine oxidase. *Biochemistry 45*, 5985–5992.
29. Kamio, M., Ko, K. C., Zheng, S. L., Wang, B. H., Collins, S. L., Gadda, G., Tai, P. C., and Derby, C. D. (2009) The chemistry of escapin: Identification and quantification of the components in the complex mixture generated by an L-amino acid oxidase in the defensive secretion of the sea snail *Aplysia californica*. *Chem.—Eur. J. 15*, 1597–1603.
30. Mattevi, A. (2006) To be or not to be an oxidase: Challenging the oxygen reactivity of flavoenzymes. *Trends Biochem. Sci. 31*, 276–283.
31. Piubelli, L., Pedotti, M., Molla, G., Feindler-Boeckh, S., Ghisla, S., Pilone, M. S., and Pollegioni, L. (2008) On the oxygen reactivity of flavoprotein oxidases: An oxygen access tunnel and gate in *Brevibacterium sterolicum* cholesterol oxidase. *J. Biol. Chem. 283*, 24738–24747.
32. Leferink, N. G. H., Fraaije, M. W., Joosten, H. J., Schaap, P. J., Mattevi, A., and Van Berkel, W. J. H. (2009) Identification of a Gatekeeper Residue That Prevents Dehydrogenases from Acting as Oxidases. *J. Biol. Chem. 284*, 4392–4397.
33. Massey, V. (1994) Activation of molecular oxygen by flavins and flavoproteins. *J. Biol. Chem. 269*, 22459–22462.
34. Roth, J. P., and Klinman, J. P. (2003) Catalysis of electron transfer during activation of O_2 by the flavoprotein glucose oxidase. *Proc. Natl. Acad. Sci. U.S.A. 100*, 62–67.
35. Roth, J. P., Wincek, R., Nodet, G., Edmondson, D. E., McIntire, W. S., and Klinman, J. P. (2004) Oxygen isotope effects on electron transfer to O_2 probed using chemically modified flavins bound to glucose oxidase. *J. Am. Chem. Soc. 126*, 15120–15131.
36. Klinman, J. P. (2007) How do enzymes activate oxygen without inactivating themselves? *Acc. Chem. Res. 40*, 325–333.
37. Gadda, G., Fan, F., and Hoang, J. V. (2006) On the contribution of the positively charged headgroup of choline to substrate binding and catalysis in the reaction catalyzed by choline oxidase. *Arch. Biochem. Biophys. 451*, 182–187.
38. Thomas, M. G., Burkart, M. D., and Walsh, C. T. (2002) Conversion of L-proline to pyrrolyl-2-carboxyl-S-PCP during undecylprodigiosin and pyoluteorin biosynthesis. *Chem. Biol. 9*, 171–184.
39. Garneau, S., Dorrestein, P. C., Kelleher, N. L., and Walsh, C. T. (2005) Characterization of the formation of the pyrrole moiety during clorobiocin and coumermycin A biosynthesis. *Biochemistry 44*, 2770–2780.